Controlling the fast electron divergence in a solid target with multiple laser pulses

L. Volpe,[1,2,*] J-L. Feugeas,[1] Ph. Nicolai,[1] J. J. Santos,[1] M. Touati,[1] J. Breil,[1] D. Batani,[1] and V. Tikhonchuk[1,†]

[1]*Univ. Bordeaux, CNRS, CEA, CELIA, UMR 5107, F-33405 Talence, France*

[2]*ELI-ALPS, ELI-Hu Nkft, Dugonics ter 13, Szeged 6720, Hungary*

(Received 8 June 2014; published 9 December 2014)

Controlling the divergence of laser-driven fast electrons is compulsory to meet the ignition requirements in the fast ignition inertial fusion scheme. It was shown recently that using two consecutive laser pulses one can improve the electron-beam collimation. In this paper we propose an extension of this method by using a sequence of several laser pulses with a gradually increasing intensity. Profiling the laser-pulse intensity opens a possibility to transfer to the electron beam a larger energy while keeping its divergence under control. We present numerical simulations performed with a radiation hydrodynamic code coupled to a reduced kinetic module. Simulation with a sequence of three laser pulses shows that the proposed method allows one to improve the efficiency of the double pulse scheme at least by a factor of 2. This promises to provide an efficient energy transport in a dense matter by a collimated beam of fast electrons, which is relevant for many applications such as ion-beam sources and could present also an interest for fast ignition inertial fusion.

DOI: 10.1103/PhysRevE.90.063108 PACS number(s): 52.38.Kd, 41.75.Jv, 52.65.Ww

I. INTRODUCTION

The study of the transport of ultrahigh intensity (UHI) laser-driven fast electrons is a subject of interest for many applications including proton-ion acceleration [1] and fast ignition inertial fusion [2]. In fast ignition approach to fusion an UHI laser is used to produce relativistic electrons which deposit their energy inside the precompressed fuel pellet. The efficiency of the laser energy coupling to the fuel is defined by the laser-electrons conversion efficiency, electron-beam mean energy, and divergence. It is estimated [3] that for a 400 g/cc fuel density, 11 kJ must be deposited within a sphere of a 15 μm radius in less then 16 ps by electrons with a mean energy of about 1.5 MeV. By using ponderomotive scaling [4] this estimate requires the laser intensities above 10^{19} W/cm^2 which are commonly reached by the current generation of UHI lasers.

In the past decades the experiments all over the world are showing that, despite the initial optimistic predictions, the laser-driven fast-electron beam is characterized by a large divergence which makes impossible to meet the fast ignition requirements. The electron-beam divergence can be controlled both by acting on the electron generation mechanism (target manufacturing technique [5]) or by controlling the electron transport (artificial confinement of the beam). Recently, a two consecutive laser-pulses scheme has been proposed by Robinson *et al.* [6] to optimize electron transport and collimation in a solid target. In this scheme two collinear laser pulses, with a given intensity ratio I_2/I_1, are used to generate energetic electron beams. The resistive azimuthal magnetic field generated by the first electron beam can guide the electron beam generated by the second pulse. This scheme has been successfully tested, in a experiment, two years later [7]. Experimental results confirmed the validity of the scheme showing that the best time delay is of the order of the laser-pulse duration. Moreover, the limits of the scheme have been demonstrated as the collimation was observed only for a special combination of the laser-pulses intensities (I_2/I_1). Indeed, a more detailed analysis shows that the electrons can be collimated in a very limited range of laser intensities and pulse durations. As was discussed in Ref. [6], exceeding intensities of 10^{20} W/cm^2 for the second laser pulse, or remaining under intensities of 10^{18} W/cm^2 for the first laser pulse, strongly reduce the efficiency of the scheme.

In this paper we propose an extension of the double pulses scheme by using a sequence of several pulses with adjusted intensity profile and delay times. An example is proposed of splitting the second (main) pulse into two pulses with the same amount of energy. Such a "triple pulses scheme" allows one to increase the total delivered laser energy by keeping the single intensity per pulse below 10^{20} W/cm^2 and stretching the whole duration of the process by only 33%. We show in the following that by using this new approach the efficiency of the scheme can be increased at least by a factor of 2, thus opening the way for future experiments on current laser devices and possible applications such as ion-beam sources.

The paper is organized as follows. In Sec. II we introduce the problem of the fast-electron generation and transport with emphasizing the role of the beam divergence. In Sec. III we describe the double pulse scheme showing experimental results and simulations. Finally, in Sec. IV we present the numerical simulations and the comparison between the double and triple pulses schemes.

II. FAST-ELECTRON-BEAM DIVERGENCE

Experiments show that the laser-driven fast-electron-beam divergence increases with the laser intensity. Green *et al.* [8] have collected the results from many experiments obtaining a scaling law of the total beam divergence (half-angle in degrees) as a function of the laser intensity (here for simplicity we assume the laser wavelength $\lambda = 1$ μm):

$$\theta_{1/2}(I_L) = 15 + 13\log\left(I_L^{18}\right), \tag{1}$$

where I_L^{18} is the laser intensity in the units of 10^{18} W/cm^2. The scaling demonstrates a gradual increase of the beam divergence

*Also at Centro de Laseres Pulsado (CLPU), Salamanca, Spain.
†volpe@celia.u-bordeaux1.fr

for the laser intensities in the range of $10^{18–20}$ W/cm^2. As was previously discussed by Debayle *et al.* in Ref. [9] both the random scattering by magnetic fields and curvature of the target surface under the action of the ponderomotive force cannot explain the observed macroscopic beam divergence. The latter can be nevertheless well described by accounting for the effect of the transverse beam velocity on the fast-electron transport. Indeed, as the laser intensity varies within the focal spot, the electrons may have a mean velocity component perpendicular to the laser propagation axis and a local propagation angle depending on the radial position. This effect contributes to the full electron divergence. The local mean propagation angle or the transverse beam velocity can modify substantially the self-generated resistive magnetic field that collimates the fast-electron beam.

The fast-electron-beam collimation due to the self-generated resistive magnetic field was studied in Ref. [10]. It was shown that this "natural collimation" is less favorable at high divergence angles, and fast-electron energies. It is inefficient at intensities in excess of 10^{19} W/cm^2. In addition as the laser intensity increases the resistive magnetic field changes its sign acting to hollow rather than to collimate the electron beam. This interpretation was proposed by Davies *et al.* [11] to explain the experimental observations of annular structures in the transverse electron-beam distribution [12]. That analysis shows that the positive (defocusing) and the negative (focusing) components of the azimuthal magnetic field are in competition depending on the value of the beam current density and the target resistivity. In the first approximation one concludes that for a given current profile (assuming a constant resistivity) the formation of a positive magnetic field depends only on the absolute value of the electron current and so on the absolute value of the laser intensity. The beam divergence is limited by the collimating magnetic field only at relatively low laser intensities.

The fast ignition approach to inertial confinement fusion requires using an electron beam with a mean energy of the order of 1.5 MeV with a transverse profile of about $\sim$15 μm at $\sim$100 μm depth [3]. These conditions can only be satisfied by collimating the beam or alternatively by reducing the initial beam divergence by modifying the composition of the target [5]. The "natural collimation" induced by the resistive magnetic field does not seem to be suitable for two reasons: (i) it works only for a small fraction of the electrons contained in the beam because the collimating magnetic field reaches the maximum intensity only at the tail of the laser pulse; (ii) it is less favorable at a high divergence angle, laser power, and fast-electron mean energy and so unfavorable at intensities in excess of 10^{19} W/cm^2 which are required for the fast ignition. It is also important to point out that the FI scheme means indeed hot and compressed targets. The electrical resistivity necessarily changes for these conditions and in consequence the magnetic fields associated to the resistivity gradients. A more detailed study on the resistivity-transient behavior can be found in [13].

III. DOUBLE PULSES SCHEME

In the "double pulses scheme" [6], the laser pulse is split in two pulses with a given intensity ratio (typically $I_2/I_1 \in$ [10:100]). The first pulse (with a moderate intensity I_1) creates an electron beam which starts to propagate inside the target. The return current generates an azimuthal magnetic field which collimates the electrons produced by the second laser pulse (with intensity I_2) arriving on the target with a given time delay. This scheme has been tested at the Rutherford Appleton Laboratory and the main results of the experiment are summarized in Ref. [7]. Figure 1 shows the half width at half maximum (HWHM) of the main electron-beam transverse size as a function of the time delay between the two pulses as was obtained in the experiment and in the hybrid kinetic simulations. These simulations show a qualitative agreement with the electron-beam HWHM measured from the images of the thermal radiation and the copper K_α emission. Let's note that the thermal spots are larger than the K_α spots due to the late time of acquisition (100 ps later than the first interaction). Indeed, as explained in Ref. [7] at that time, an expanding plasma is present at the rear side of the target.

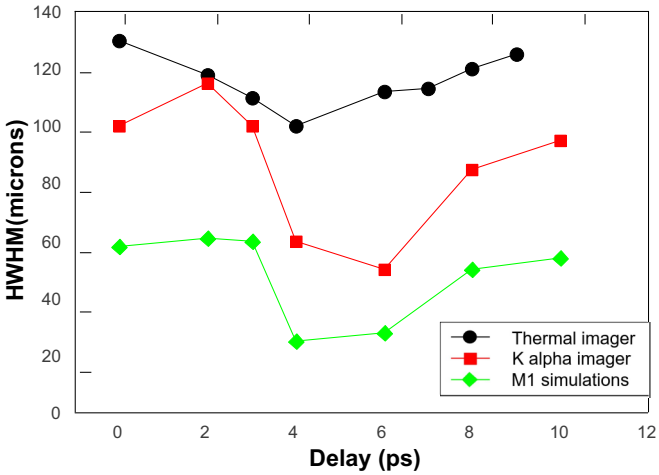

FIG. 1. (Color online) Dependence of the HWHM of the Cu K_α (red squares) and thermal emission images (black dots) from the rear target surface on the time delay compared with (green diamonds) numerical simulations. Copied with permission from Scott [7].

In the double pulses scheme, the resistive magnetic field created by the first electron beam starts to collimate the incoming second electron beam immediately upon the second pulse arrival. The collimation of the second beam induces a significant steepening of the current density profile, which, in turn, increases the total resistive magnetic-field intensity. The induced magnetic field increases in magnitude and moves deeper into the target, then it diffuses radially, reducing in magnitude.

A. Numerical simulations

The fast electron propagation through the target has been modeled with the radiation hydrodynamic code CHIC coupled to the kinetic module $M1$ [14,15]. This fast kinetic model describes the collisional transport of energetic particles while taking into account the self-generated magnetic field. Derived from the Vlasov-Fokker-Planck equation, it involves an angular closure in the phase space leading to a set of hyperbolic equations for the moments of the distribution function evolving

in time, space, and energy. This method is suitable for the computation of the fast electron transport on the hydrodynamic time scales. It provides an alternative to prohibitive full kinetic simulations with large, complex, and time consuming codes.

Simulations have been performed in a cylindrical geometry (where z is the beam propagation axis and r is the radial direction in the target surface plane). The target is a 96-μm-thick (along the z direction) aluminium cylinder of radius of 96 μm. The simulations were conducted with 4 μm resolution. Initial conditions have been calculated assuming Beg [Eq. (2) and Ref. [16]] and Wilks [Eq. (3) and Ref. [4]] scaling laws for the estimate of the fast-electron mean energy as a function of the laser intensity and the Solodow scaling law [Eq. (4), Ref. [17]] to account for the laser-electron conversion efficiency ξ as a function of the laser intensity:

$$T_b = \alpha_b\left(\lambda^2 I_L^{18}\right)^{1/3}, \quad \alpha_b = 215, \tag{2}$$

$$T_w = \alpha_w\left(\sqrt{1+\lambda^2 I_L^{18}/2.8}-1\right), \quad \alpha_w = 511, \tag{3}$$

$$\xi = \alpha_s\left(\lambda^2 I_L^{18}\right)^{1/4}, \quad \alpha_s = 0.108, \tag{4}$$

where T_b and T_w are in keV, and the laser intensity I_L is in 10^{18} W/cm^2. We have chosen $T_e = \max[T_b, T_w]$ and the initial electron-beam distribution is represented as follows:

$$F(r,z,E,\theta) = G^1_{w_t}(t)\Omega_{\Delta\theta_0}(\theta_p(r))G^n_{w_r}(r)M_{T_e}(E), \tag{5}$$

where

$$G^n_w(x) = \exp\{-\ln(2)(x/w)^{2n}\} \tag{6}$$

is a super-Gaussian function, w is the HWHM, and n is the super-Gaussian degree ($n = 1$ Gaussian). The function $G^1_{w_t}(t)$ describes the time profile, $G^n_{w_r}(r)$ is the radial profile, and $M_{T_e}(E) = \sqrt{E}e^{-E/T_e}$ is the Maxwellian energy distribution. The angular distribution is given by

$$\Omega_{\Delta\theta_0}(\theta_p(r)) = \tfrac{1}{2}[\cos(\Delta\theta_0)+1]\cos(\theta_p(r)), \tag{7}$$

where

$$\theta_p(r) = \min[\theta_{\max}(r/w_e)^b, \theta_{\max}], \quad 1 < b < 2 \tag{8}$$

is the local electron mean propagation angle and $\Delta\theta_0$ is the local dispersion angle. As it was shown in Ref. [9], by assuming that at the normal incidence the $\vec{J}\times\vec{B}$ heating [4] is the dominant process, it is possible to connect the parameter b with the slope of the radial profile n. Indeed, starting from the ponderomotive force, the electron transverse and longitudinal momenta can be written as $p_r \propto \partial_r I_L(r)/\gamma$ and $p_z \propto I_L(r)/\gamma$ (where γ is the electron relativistic factor). Then the mean propagation angle can be expressed as $\tan\theta(r) = p_x/p_z \propto \partial_r I_L(r)/I_L(r)$, and those $\theta(r) = \tan^{-1}(r/w)^{2n}$. The formation and the intensity of the resistive B_θ field depends strongly on the parameters n and b. This can be demonstrated by solving the Faraday equation for the magnetic field in the "rigid model" approximation [11] $|B_\theta| \propto n(r/w_e)^{(2n)}$ (see the Appendix for the detailed explanation).

Figure 2 shows an example of the magnetic-field distribution for a given case at different values of b and at a fixed time. It contains two lobes. The negative magnetic field near the axis focuses the central part of the beam. In contrast, the outer part of the beam is defocused by the positive lobe of the

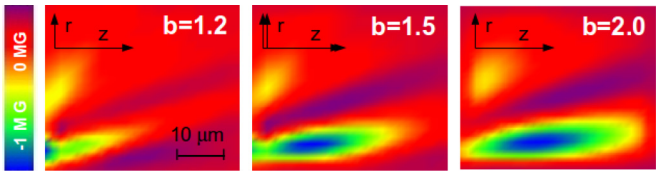

FIG. 2. (Color online) Spatial distribution of the magnetic field B_θ for the values of the parameter b increasing from the left ($b = 1.2$) to the right ($b = 2.0$) at the time of the magnetic-field maximum.

magnetic field. The beam parameter b controls the position where the magnetic field changes its sign. Decreasing the b parameter (in Fig. 2 from the right to the left) the negative (focusing) component of B_θ is reduced, while the positive one (defocusing) grows around the center of the beam ($r \simeq 0$).

To account for the laser-electrons conversion efficiency we represent the laser intensity as

$$I_L(r,t,n,w_L,w_t) = I_L G^n_{w_L}(r)G^1_{w_t}(t). \tag{9}$$

The total delivered laser energy is given by

$$E_L = \int_0^\infty\int_{-\infty}^\infty I_L(r,t,n,w_L,w_t)2\pi r\,dr\,dt \tag{10}$$

$$= I_L\int_0^\infty G^n_w(r)2\pi r\,dr\int_{-\infty}^\infty G^1_{w_t}(t)dt \tag{11}$$

$$= I_L{}^n F_{w_L} F_{w_t}, \tag{12}$$

where ${}^nF_w = 2\pi\int_R G^n_w(r)r\,dr = \pi\Gamma(1/n)/\ln(2)^{1/n}w^2$, $\Gamma(z) = \int_0^\infty t^{z-1}e^{-z}dt$ is the Euler gamma function, and $F_w = \int_R G^1_w(t)dt = \sqrt{\pi/\ln(2)}w$.

The intensity of the laser-generated electron beam

$$I_e(r,t,n,w_e,w_t) = I_e G^n_{w_e}(r)G^1_{w_t}(t) \tag{13}$$

is calculated introducing an arbitrary parameter $I_{\rm cut}$ which represents the minimum intensity required to produce fast electrons. With this assumption the spatial HWHM w_e and the peak intensity I_e of the laser-generated electron beam are given by

$$w_e = \delta w_L, \quad \delta = \ln(I_L/I_{\rm cut})^{1/2n}, \tag{14}$$

$$I_e = \alpha_l\alpha_s I_L^{5/4}/\delta^2, \quad \alpha_l = \int_0^{w_L} I_L r\,dr \Big/ \int_0^\infty I_L r\,dr, \tag{15}$$

where α_l represents the fraction of the total laser energy within the HWHM. As an example, the intensities of 10^{19-20} W/cm^2 correspond to $\delta = 3$–4 with $n = 0.7$. Finally, the total electron-beam energy is given by

$$E_e = \alpha_I I_L^{5/4}, \quad \alpha_I = \alpha_s\alpha_w{}^n F_{w_e} F_{w_t}, \tag{16}$$

$$E_e = \alpha_e E_L^{5/4}, \quad \alpha_e = \frac{\alpha_s\alpha_w{}^n F_{w_e}}{{}^nF_{w_L}^{5/4}F_{w_t}^{1/4}}. \tag{17}$$

The electron-beam intensity and the mean temperature are estimated, as functions of the laser parameters, by injecting Eqs. (16) and (17) into Eqs. (2), (3), and (15).

B. Parametric analysis of the beam guiding

In this section we present the results of numerical simulations performed to study the double pulse scheme [6], its stability, and possible modifications. In particular, it is shown that equally sharing the amount of energy of the second (main) pulse in two consecutive pulses, one can improve the efficiency of beam guiding. Collecting all the energy in a single pulse (the second one in the double pulse scheme) is convenient in terms of the laser-electron conversion efficiency, which increases with the intensity [18]. However, it is not so from the point of view of guiding. By increasing the laser intensity one reduces the collimating magnetic field [10] and increases the total electron-beam divergence [8]. The triple pulse scheme overcomes these problems and opens the way for a more efficient beam guiding.

1. Double pulses scheme

Here we present several examples which are important for understanding the physics of beam guiding. The first example concerns the time dependence of the maximum magnetic field B_θ. The simulations have shown that for laser intensities in the range of 10^{19-20} W/cm^2 the time of maximum magnetic field depends only on the laser-pulse duration and the electron-beam size w_e:

$$t_{\text{best}} = s(w_e)w_t + 0.7, \tag{18}$$

where w_t is the pulse time HWHM in picosecond and $s(w_e) = 0.157w_e + 0.9$ is a dimensionless parameter related to the electron-beam size in μm. Assuming $w_e = 17$ μm, and $w_t = 1$ ps (these are the conditions in Ref. [7]) we obtain $s = 3.6$ and then $t_{\text{best}} = 4.3$ ps. The same calculation by assuming $w_e = 10$ μm, and $w_t = 0.4$ ps gives $s = 2.5$ and a shorter $t_{\text{best}} = 1.7$ ps. Finally, t_{best} can be reduced both by reducing the pulse duration (i.e., w_t) and the electron-beam size (i.e., s). The beam size dependence of t_{best} can be understood also by solving the equation $\partial B_\theta(t)/\partial t = 0$ in the "rigid model" approximation (see the Appendix). In conclusion, both numerical simulations and experimental results suggest that the best time delay between the consecutive pulses is defined as $\Delta_t \simeq t_{\text{best}}$ with an uncertainly of about 1 ps. Delays shorter (the magnetic field is still not at its maximum) or longer (the magnetic field is decreasing due to the diffusion) than t_{best} reduce the efficiency of the double pulses scheme. Figure 3 (left panel) shows the maximum B_θ as a function of time in the double pulses scheme at various time delays between the first and the second pulses. The continuous and the dotted blue lines represent respectively the maximum magnetic field and the main laser beam temporal profile alone (i.e., without the first pulse). The azure line represents (up to 10 ps) the maximum magnetic field of the first pulse which is amplified by the injection of the second pulse at different time delays, the green line $\Delta t = 3$ ps, red line $\Delta t = 4$ ps, and azure line $\Delta t = 8$ ps. At the best condition the magnetic field propagates along the beam axis "driving" the electrons inside the target.

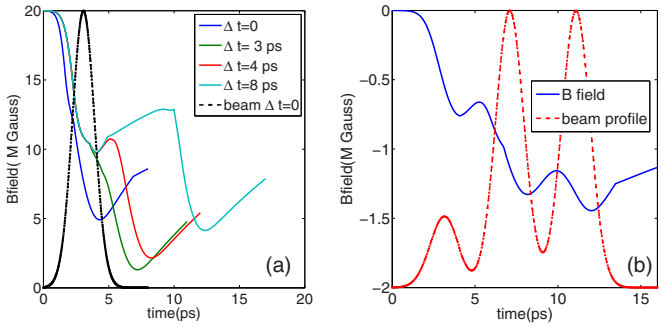

FIG. 3. (Color online) (a) Temporal evolution of the maximum magnetic field at various time delays between the first and the second laser pulse. The blue line (first from left) $\Delta t = 0$ ps represents the second pulse alone. The azure line (the line arriving till 18 ps) represents (up to 10 ps) the maximum magnetic field of the first pulse which is amplified by the injection of the second pulse at different time delays, green line (second from left) $\Delta t = 3$ ps, red line (third from left) $\Delta t = 4$ ps, and azure line (fourth from left) $\Delta t = 8$ ps. The diffusion time of the magnetic field depends only on the beam radius and on the target resistivity $\tau_{B_\theta} \sim w_e^2/\eta$. (b) Temporal evolution of the maximum magnetic field (continuous line) and of the laser-pulse intensity (dotted line) for the time delay $\Delta t = 4$ ps for the triple pulses scheme.

The main problem of the electron guiding is that the electron-beam divergence increases with the laser intensity. Consequently, the "natural collimation" becomes less and less efficient, as it traps in the guiding channel only a small paraxial part of the beam. Double pulses scheme overcomes this problem but still it is limited to laser intensities smaller than 10^{20} W/cm^2. Reference [6] shows that this limitation is due to the interplay between the strength of the resistive magnetic field generated by the first electron beam and the momentum of the incoming electrons of the second beam. According to [6], the guiding imposes a condition on the radial extension R and on the absolute value of the negative magnetic field B_θ generated by the return current of the first electron beam. This condition writes

$$R \geqslant r_L, \quad \text{where} \quad r_L = \frac{\gamma v_e m_e}{e|B_\theta|}(1 - \cos\theta_{1/2}) \tag{19}$$

is the Larmor radius and e, m_e, v_e, γ respectively the charge, mass, velocity, relativistic factor of the electrons generated by the second laser pulses and $\theta_{1/2}$ is given by Eq. (1). This condition can also be written (by assuming $\lambda = 1$ μm) in terms of laser and target parameters only:

$$I_1^{18} > 1.6\times10^{-3}\left(\frac{1-\cos\theta_{1/2}}{\eta[\mu\Omega\,\text{m}]\xi\, w_t^1[\text{ps}]}\right)^{3/2}\left(I_2^{18}\right)^{3/4}, \tag{20}$$

where η is the target resistivity and w_t^1 represent the HWHM of the first laser pulse. Assuming [6] $\eta = 0.8$, $w_t^1 = 0.25$, and $\xi = 0.2$ [see Eq. (4)] we get

$$I_1^{18} > 0.2\left(I_2^{18}\right)^{3/4}. \tag{21}$$

According to this condition one may increase the intensity of the first laser beam and consequently reduce the intensity of the second one by keeping the total energy constant. Since a part of electrons produced by the first laser pulse will be lost (all the electrons produced before the magnetic field attains

TABLE I. Comparison between double (case A) and triple (case B) pulses scheme.

(A) Two pulses configuration									
	E_L (J)	w_t (ps)	w_L (μm)	n_L (/)	I_L (W/cm^2)	E_e (J)	T_e (MeV)	ξ (/)	$\theta_{1/2}$ (deg)
I beam	15	1	3.5	0.6	5×10^{18}	1	0.4	0.15	12°
II beam	175	1	3.5	0.6	10^{20}	40	2.5	0.34	21°
(B) Three pulses configuration									
	E_L (J)	w_t (ps)	w_L (μm)	n_L (/)	I_L (W/cm^2)	E_e (J)	T_e (MeV)	ξ (/)	$\theta_{1/2}$ (deg)
I beam	15	1	3.5	0.6	8×10^{18}	1	0.4	0.15	12°
II beam	87	1	3.5	0.6	5×10^{19}	18	1.7	0.29	17°
III beam	87	1	3.5	0.6	5×10^{19}	18	1.7	0.29	17°

its maximum value), this solution is not favorable. The second possibility is to reduce the intensity of the second beam by stretching it in time. As the laser beam intensity is defined by the required electron energy, this stretching can be achieved by splitting the second laser pulse in a sequence of pulses separated by the appropriate time delays.

According to Eq. (21) and assuming $I_2 = 10^{20}$ W/cm^2 we get $I_1 > 3\times10^{18}$ W/cm^2. Let us now split the second pulse into two equal pulses having a twice lower intensity. This will relax the condition (20) by a factor of $2^{3/4}$; in addition the intensity reduction induces a reduction of the electron-beam divergence (from $\theta_{1/2} \simeq 20°$ to $\theta_{1/2} \simeq 15°$) again by a factor $2^{3/4}$ [according to Eq. (1)]. Thus by reducing the intensity by a factor of 2 one can achieve a significant relaxation of the condition (20) by a factor larger than 2 (see in the following). This simple example is confirmed by numerical simulations.

2. *Triple pulses scheme*

We limit ourselves here by splitting the second pulse into two pulses of equal intensities. As shown in Fig. 3 (right panel) in the triple pulses scheme the third laser pulse is injected when the magnetic field due to the first two pulses achieves its maximum. In this case simulations show that the delay times shorter than $t_{\rm best}$ are preferable. This is explained by the fact that the magnetic field of the second beam starts to follow the electron beam along the propagation direction moving away from the front target surface. In the following, three configurations are compared

(A) Double pulses configuration: the first pulse ($w_t = 1$ ps) with a moderate energy (10%) followed by the second pulses ($w_t = 1$ ps) carrying out the rest (90%) of the energy. The total duration of the process is ∼12 ps.

(B) Triple pulses configuration: the first pulse ($w_t = 1$ ps) with a moderate energy (10%) followed by two pulses ($w_t = 1$ ps) each of them carrying out half of the remaining (45% + 45%) energy. The total duration of the process is ∼16 ps.

(C) Single pulse configuration: the single pulse ($w_t = 1$ ps) with the same energy as the second pulse in case A (total duration of the process is ∼6 ps).

We choose configuration A such that the collimation condition (20) is not satisfied ($I_2 \sim 10^{20}$ W/cm^2). Consequently, the configuration B is obtained by equally sharing the energy in the second and third pulses $I_2 \sim I_3 \sim 5\times10^{19}$ W/cm^2. The laser parameters for configurations A and B are chosen according to the typical values of the Vulcan laser at the Rutherford Appleton Laboratory which has been used to test the double pulses scheme [7]. The total available energy is $E_L = 190$ J; the pulse duration $w_t = 1$ ps HWHM the laser pulses are focused on a 96-μm-thick aluminium target within a focal spot of $w_L = 3.5$ μm radius. Starting from E_L, w_t, w_L and assuming $n = 0.6$ one may calculate all the parameters by using Eqs. (3)–(17). The laser and electron-beam parameters for the configurations A and B are listed in Table I.

Figure 4 shows the distribution of the electron-beam density for the single pulse (case C) at $t = 6$ ps, for the double pulse scheme (case A) at $t = 10$ ps and for the triple pulses scheme (case B) at $t = 13$ ps. As the double pulses parameters do not fulfill the collimation condition the beam strongly diverges in the case A. It would be possible assuming a lower intensity for the second pulse to obtain a good electron-beam collimation but the electron energy will be lower. The triple pulses scheme allows one to guide the electrons with the required energy.

Since the experimental results are often presented with 2D images obtained by collecting the K_α emission coming from the interaction of the fast-electron beam with a control layer we have calculated the time integrated K_α emission from the fast-electron beam by assuming that the Copper tracer is distributed homogeneously in the aluminium target. Such an "equivalent Cu K_α" distribution better represents the electron-beam distribution and can be compared with the real experimental observation.

Figure 5 shows the distribution of the resistive magnetic field and of the Cu K_α emission at two time instants ($t = 6$,

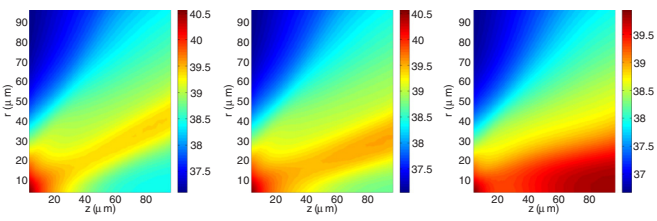

FIG. 4. (Color online) Distribution of the electron-beam density ($\log n_e$) at the end of the process for the double pulse scheme at $t = 10$ ps (case A, center) and for the triple pulses scheme at $t = 13$ ps (case B, right). In the left panel is shown the case C with the energy $E = 40$ J. Other parameters are shown in Table I.

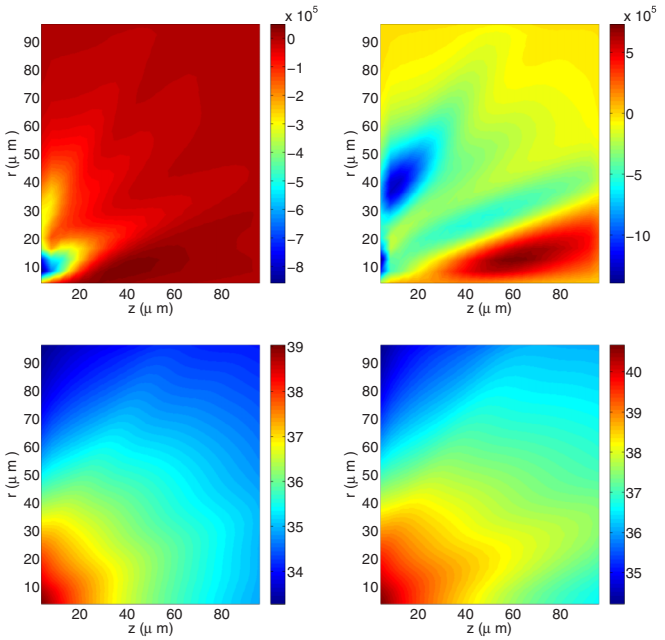

FIG. 5. (Color online) Distribution of the resistive magnetic field ($\log B_\theta$; top line from left $t = 6{,}10$ ps) and the K_α emission ($\log K_\alpha$; bottom line from left $t = 6{,}10$ ps) for the case A.

10 ps for the magnetic field and $t = 6{,}12$ ps for the Cu K_α signal) for the case A (with 96-μm-thick target). These images must be compared with that obtained for the case B in Fig. 6 at the time instants ($t = 6{,}14$ ps for the magnetic field and $t = 6{,}16$ ps for the Cu K_α signal).

A comparison of these figures shows that the three pulses scheme is more efficient. Indeed as shown in Fig. 6 the K_α

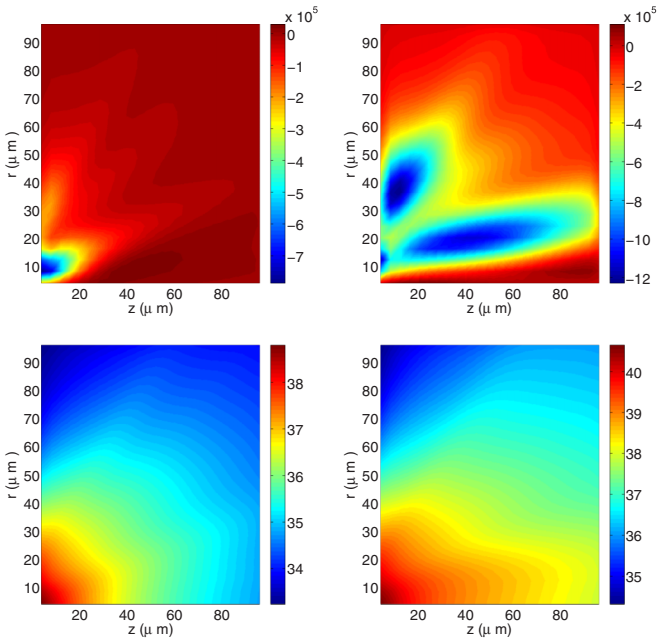

FIG. 6. (Color online) Distribution of the resistive magnetic field ($\log B_\theta$; top line from left $t = 6{,}14$ ps) and the K_α emission ($\log K_\alpha$; bottom line from left $t = 6{,}14$ ps) for the case B.

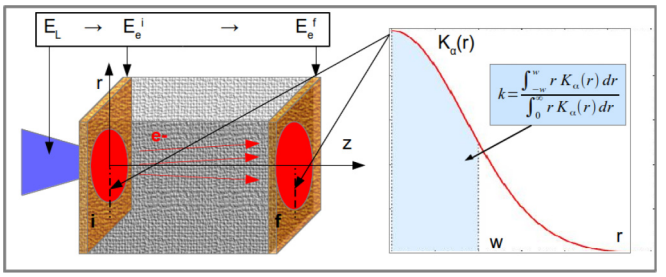

FIG. 7. (Color online) (left) Scheme of a "typical" experiment with the target having two tracer layers at the front and at the rear side. (Right) Radial line out of the K_α signal coming from the tracer layers.

signal is better confined along the propagation axis and the negative part of the resistive magnetic field can collimate the electrons. In contrast, the positive part (that hollows the beam) is much less important. This is not the case in the double pulse scheme (Fig. 5) where the K_α signal is much wider radially and the competition between the negative and the positive part of the resistive magnetic field leads to a significant modification of the beam spatial distribution with a smaller number of guided electrons. The negative component of the magnetic field pushes electrons towards higher beam current density regions despite the positive component which does the opposite. The combination of these two processes leads to a macroscopic electron-beam "filamentation."

In order to better compare the efficiencies of the double (A) and triple (B) pulses scheme we consider a "conventional" experimental setup shown in Fig. 7. The target is covered by two thin tracer copper layers, one at the front (i) and another at the rear (f) side of the target. Then $K_\alpha^{(i,f)}(r)$, $w^{i,f}$, and $k^{i,f}$ represent respectively the radial profile, the HWHM, and the normalized integrated copper K_α emission measured at the front and at the rear side of the target. The incident electron-beam transverse HWHM is $w_i = 20$ μm (for all the cases). Following this scheme we define three types of indices: the first two types for the estimate of the beam collimation and compression degree and the latter for the estimate of the laser-electrons conversion efficiency. In particular, as follows.

(1) Collimation degree indices. (i) $w_x^{f/i} = w_x^f / w_x^i$ is the ratio between the K_α signal size measured at the rear and at the front side of the target ($x =$ A,B,C). (ii) $w_{x/C}^f = w_x^f / w_C^f$ is the ratio between the K_α signal size measured at the rear side of the target in the case $x =$ A/B vs C.

(2) Compression degree indices. (iii) $k_x^{f/i} = k_x^f / k_x^i$ is the ratio between the normalized integrated within HWHM K_α signal measured at the rear and at the front side of the target ($x =$ A,B,C). (iv) $k_{x/C}^f = k_x^f / k_C^i$ is the ratio between the normalized integrated within HWHM K_α signal measured at the rear side of the target in the case $x =$ A/B vs C.

(3) Laser-electrons conversion efficiency. (v) $\epsilon^{i/L} = E_e^i / E_L$ is the laser-electron-beam conversion efficiency at the front side of the target. (vi) $\epsilon^{f/i} = E_e^f / E_e^i$ is the electron-beam transport efficiency from the front to the rear side of the target. (vii) $\epsilon^{f/L} = E_e^f / E_L$ is the laser-electron-beam conversion and transport efficiency at the rear side of the target ($\epsilon^{f/L} = \epsilon^{f/i} \cdot \epsilon^{i/L}$).

TABLE II. Collimation [(i),(ii)], compression [(iii),(iv)], and conversion efficiency [(v),(vi),(vii)] indices for the cases A and B compared with the single pulse case C.

	(i) $w_x^{f/i}$	(ii) $w_{x/C}^{f}$	(iii) $k_x^{f/i}$	(iv) $k_{x/C}^{f}$	(v) $\epsilon_x^{i/L}$	(vi) $\epsilon^{f/i}$	(vii) $\epsilon_x^{f/L}$
A	3	0.86	0.35	1.5	0.21	0.031	0.006
B	2	0.57	0.65	2.8	0.19	0.063	0.012

The collimation parameter describes the reduction of the beam size and the compression parameter accounts for the reduction of the beam size while keeping the total number of particles constant. A good beam collimation does not necessarily imply a good beam compression. For that we consider separately the collimation, that is connected to the beam size only w_e, and the compression, which gives also information of the number of confined electrons (i.e., K_α signal yield).

The above-mentioned indices are calculated for the cases A (double pulses), B (triple pulses), and C (single pulses) and the results are listed in Table II. The indices from (ii) to (iv) confirm a doubling of the collimation and compression degree for the case of the triple pulses scheme compared to the double pulses scheme. The indices from (v) to (vii) confirm this trend in terms of the conversion efficiency. In particular, the index (v) shows that the conversion efficiency of the laser to electrons decreases in the triple pulses scheme according to the fact that lower laser intensities correspond to a lower conversion efficiency. The difference between the two schemes appears clearly in the index (vi) which gives an estimate of the efficiency of the electron-beam transport from the front to the rear side of the target; this efficiency is doubled for the triple pulses scheme as shown in Table II.

IV. CONCLUSIONS AND PROSPECTIVES

In conclusion, we propose an extension of the double pulses scheme allowing one to increase the efficiency of fast-electron-beam transport in a dense plasma. Simulations show that the multiple pulses scheme is more flexible, allowing one to overcome several limitations already observed in the experiments. In particular, by increasing the number of pulses (and then the duration of the process) one can reduce the single pulse intensity while keeping the total delivered energy constant and the total duration of the process within the fast ignition limits. The presented example of three consecutive pulses shows that the efficiency of the double pulse scheme can be increased at least by a factor of 2. Moreover, putting together many laser pulses gives a possibility to increase the total amount of delivered energy while keeping the average energy constant. This method is promising to achieving an efficient energy transport in a dense matter by a collimated beam of fast electrons, which is relevant for many applications such as fast ignition inertial fusion and ion beam sources. Although the magnetic guiding improves the electron transport there are several points that need a further optimization. First, the laser-electron coupling efficiency is a relatively low 30% [see Eq. (4)] and needs to be improved. It can be done by appropriate shaping of the laser prepulse and forming a preplasma. This issue is not in the scope of the present study. Second, the triple pulse scheme allows one to transport more than 50% of the produced fast electrons in a form of a collimated beam over a distance about 100 μm. This is a significant improvement compared to the one or two pulses but it is still insufficient for the fast ignition. It would be interesting to find additional processes that may allow one to guide the remaining 50% of fast electrons.

ACKNOWLEDGMENTS

The work presented here was performed under financial support from the Aquitaine Regional Council through Project ARIEL 2012, and both the French National Agency for Research (ANR) and the competitiveness cluster Alpha-Route des Lasers through Project TERRE No. ANR-2011-BS04-014. This study has been carried out in the frame of the Investments for the future Programme IdEx Bordeaux LAPHIA (No. ANR-10-IDEX-03-02). The authors are thankful to A. Morace for helpful discussions.

APPENDIX: RIGID MODEL

The "rigid model" of the magnetic-field generation by a high current electron beam assumes that the electron-beam current J is given and it is completely compensated by the return current of plasma electrons $J + J_t \sim 0$. The electric field is produced due to the plasma resistivity η according to Ohm's law

$$\vec{E} = \eta \vec{J}_t. \tag{A1}$$

The target resistivity is supposed to depend on the plasma temperature according to the power law

$$\eta = \eta_0 \frac{T}{T_0}^{\alpha}, \tag{A2}$$

which evolves in time because of Ohm's heating

$$\frac{\partial T}{\partial t} = \frac{\eta J_t^2}{C_v}, \tag{A3}$$

where C_v is a constant heat capacity. The time evolution of the magnetic field is defined by Faraday's law:

$$\frac{\partial B}{\partial t} = \eta \vec{\nabla} \times \vec{J} + \vec{\nabla} \eta \times \vec{J}. \tag{A4}$$

Here the first term in the right-hand side is a source of an azimuthal magnetic field that pushes ($B < 0$) electrons towards regions of a higher current density causing collimation of the electron beam. The second term in the right-hand side is a source of a magnetic field that pushes ($B < 0$) electrons towards regions of higher resistivity leading to the electron beam hollowing. Assuming a super-Gaussian profile for the electron-beam current

$$J = -J^0 e^{-\ln(2)\left(\frac{r}{w_e}\right)^{2n}}, \tag{A5}$$

the solution of Eq. (A4) can be written as

$$B_\theta = 2n\left(\frac{r}{w_e}\right)^{(2n-1)}\frac{CT_0}{J} \times\left[1+\frac{1+\alpha}{1-\alpha}\left(\frac{T}{T_0}\right)+\frac{2}{1-\alpha}\left(\frac{T}{T_0}\right)^{\alpha}\right], \quad \text{(A6)}$$

$$T = T_0[1+(1-\alpha\tau)]^{1/(1-\alpha)}, \quad \alpha < 1, \quad \text{(A7)}$$

where $\tau = (\eta_0 J^2)(CT_0)t$.

1. Beam hollowing

The above solution for the magnetic field shows that it depends strongly on the radial shape of the electron beam (n) and the plasma temperature T. It has been shown [11] that if the resistivity falls faster than linearly with the temperature ($\alpha < -1$) then the magnetic field can change the sign acting to hollow rather than to focus the electron beam. In particular, assuming the Spitzer regime (i.e., $\alpha = -3/2$), the beam hollowing appears for $\tau > 17$ as shown in Fig. 8.

The positive part of the magnetic field grows up at the center of the electron beam and then acts to hollow the beam. It was shown [11] that for the typical conditions (the target made of a mylar with the electron density $n_e = 4.4\times10^{29}$ m^{-3}; the laser wavelength $\lambda = 1$ μm; the Spitzer resistivity with $Z\ln\Lambda \sim 10$ and $\eta_0 = 2$ Ω m; the laser to electrons conversion efficiency $\sim$0.3) the electron-beam hollowing appears for laser intensities larger than 10^{18} W/cm^2.

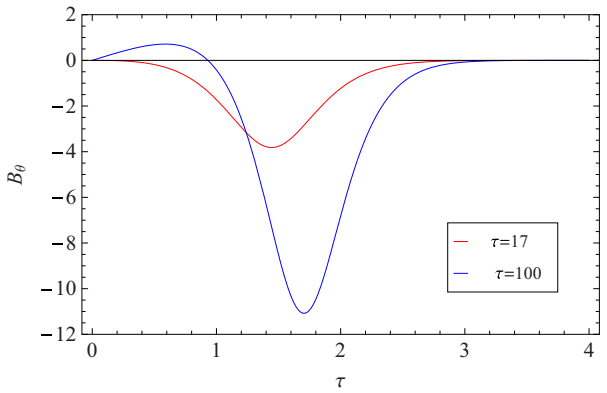

FIG. 8. (Color online) Magnetic field (in arbitrary units) radial profile as obtained from Eq. (A8) for two cases $\tau = 17$ (max $B \sim -4$) (no hollowing) and $\tau = 100$ (max $B \sim -11$).

2. Time evolution of the negative magnetic field

It is important to give an estimate of the time t_h when the negative part (focusing) of the magnetic field reaches maximum. This can be done by equating Eq. (A4) to zero (assuming the Spitzer regime $\alpha = -3/2$):

$$\frac{\partial B}{\partial t} = 2n\left(\frac{r}{w_e}\right)^{(2n-1)}\frac{CT'}{5J}\left[6\left(\frac{T}{T_0}\right)^{-5/2}-1\right] = 0. \quad \text{(A8)}$$

For a given radial position (i.e., $r = w_e$) and by using Eq. (A8) one finds $\tau = 10$ and then

$$t_h = \frac{10CT_0}{\eta_0 J^2}. \quad \text{(A9)}$$

[1] E. L. Clark *et al.*, Phys. Rev. Lett. **84**, 670 (2000).
[2] M. Tabak, J. Hammer, M. E. Glinsky, W. L. Kruer, S. C. Wilks, J. Woodworth, E. M. Campbell, M. D. Perry, and R. J. Mason, Phys. Plasmas **1**, 1626 (1994).
[3] S. Atzeni, Phys. Plasmas **6**, 3316 (1999).
[4] S. C. Wilks, W. L. Kruer, M. Tabak, and A. B. Langdon, Phys. Rev. Lett. **69**, 1383 (1992).
[5] A. Debayle, L. Gremillet, J. J. Honrubia, and E. d'Humieres, Phys. Plasmas **20**, 013109 (2013).
[6] A. P. L. Robinson, M. Sherlock, and P. A. Norreys, Phys. Rev. Lett. **100**, 025002 (2008).
[7] R. H. H. Scott *et al.*, Phys. Rev. Lett. **109**, 015001 (2012).
[8] J. S. Green *et al.*, Phys. Rev. Lett. **100**, 015003 (2008).
[9] A. Debayle, J. J. Honrubia, E. d'Humières, and V. T. Tikhonchuk, Phys. Rev. E **82**, 036405 (2010).
[10] A. R. Bell and R. J. Kingham, Phys. Rev. Lett. **91**, 035003 (2003).
[11] J. R. Davies *et al.*, Plasma Phys. Control. Fusion **48**, 1181 (2006).
[12] P. A. Norreys *et al.*, Plasma Phys. Control. Fusion **48**, L11 (2006).
[13] B. Vauzour, A. Debayle, X. Vaisseau, S. Hulin, H.-P. Schlenvoigt, D. Batani, S. D. Baton, J. J. Honrubia, Ph. Nicolaï, F. N. Beg, R. Benocci, S. Chawla, M. Coury, F. Dorchies, C. Fourment, E. d'Humières, L. C. Jarrot, P. McKenna, Y. J. Rhee, V. T. Tikhonchuk, L. Volpe, V. Yahia, and J. Santos, Phys. Plasmas **21**, 033101 (2014).
[14] Ph. Nicolaï, J.-L. Feugeas, C. Regan, M. Olazabal-Loumé, J. Breil, B. Dubroca, J.-P. Morreeuw, and V. Tikhonchuk, Phys. Rev. E **84**, 016402 (2011).
[15] M. Touati, J.-L. Feugeas, Ph. Nicolaï, J. J. Santos, L. Gremillet, and V. T. Tikhonchuk, New J. Phys. **16**, 073014 (2014).
[16] F. N. Beg, A. R. Bell, A. E. Dangor, C. N. Danson, A. P. Fews, M. E. Glinsky, B. A. Hammel, P. Lee, P. A. Norreys, and M. Tatarakis, Phys. Plasmas **4**, 447 (1997).
[17] A. A. Solodov, K. S. Anderson, R. Betti, V. Gotcheva, J. Myatt, J. A. Delettrez, S. Skupsky, W. Theobald, and C. Stoeckl, Phys. Plasmas **16**, 056309 (2009).
[18] L. Volpe, D. Batani, A. Morace, and J. J. Santos, Phys. Plasmas **20**, 013104 (2013).